PHYSICAL REVIEW B VOLUME 26, NUMBER 11 1 DECEMBER 1982

Order and deterministic chaos in hard-disk arrays

Michael Rubinstein and David R. Nelson
Department of Physics, Harvard University, Cambridge, Massachusetts 02138
(Received 27 May 1982)

Order in computer-generated binary arrays of hard disks grown from a seed cluster is studied. As the composition and ratio of disk diameters are varied, we find both crystalline and amorphous samples, as well as "hexatic" configurations with short-range translational order but extended orientational correlations. A single impurity disk placed at the center of an otherwise homogeneous array traps dislocations and disclinations when its diameter deviates sufficiently from that of the disks packed deterministically around it. For still larger deviations, the impurity disk gives rise to chaotic arrays of stacking faults and grain boundaries. An alternative spiral packing algorithm leads to a particularly simple transition from order to deterministic chaos. The ratio of disk diameters plays the role of a control parameter.

I. INTRODUCTION

Dense random-packing models of identical particles have been under active investigation for over 20 years. Although conceived initially as models of dense liquids,[1] they now appear relevant as structural models of metallic glasses.[2,3] An important topological feature of these packings is a tendency to maximize the local density by forming tetrahedral clusters. Because tetrahedra cannot be close packed to fill space, highly frustrated, or "jammed," particle configurations result. Radial distribution functions deduced from dense random-packing models agree well with diffraction experiments on metallic glasses,[2] despite the fact that two different particle sizes are required to obtain stable glasses in the laboratory.[4]

The situation is quite different in two dimensions,[5] where triangular packing units not only maximize the local density, but also combine neatly into a space-filling lattice. Here, one can impose a controllable amount of randomness via a finite concentration of particles with the "wrong" diameter. Following early work by Nowick and Mader,[6] randomly packed planar arrays of ball bearings with two different sizes were studied by Nelson, Rubinstein, and Spaepen.[7] Translational and orientational order parameters useful in studies of equilibrium melting[8] were used to characterize the degree of disorder in various arrays. For dilute concentrations of large spheres imbedded in a matrix of smaller ones, the resulting configurations displayed short-range translational order, but extended correlations in the orientation of local crystallographic axes. Such packings are a quenched analog of the equilibrium hexatic phase, and result from the tendency of large spheres to trap dislocations. Depending on the relative concentration of large and small spheres, and on the ratio of sphere diameters, one also finds completely amorphous configurations (with short-range translational and orientational order), as well as packings whose crystalline order is disrupted by networks of grain boundaries.

In this paper we study similar questions in arrays of hard disks generated on a computer via a simple deterministic packing algorithm. The procedure is a two-dimensional version of one used by Bennett[9] to study packings of uniform hard spheres: Successive particles are brought into contact with a growing cluster subject to the condition that they be as close as possible to the center of an initial-seed configuration. The method has the advantage that it is extremely easy to produce packings with large numbers of particles, and that the resulting three-dimensional radial distribution functions agree rather well with large annealed ball bearing packings investigated by Finney.[10] Although the extrapolated density is 4% lower than Finney's value, the "global" algorithm described above works considerably better than a more "local" packing criterion also studied by Bennett.[9]

Order in any two-dimensional structure is conveniently characterized by translational and orientational correlation functions. A complex translational order parameter,

$$\rho_{\vec{q}}(\vec{r}_j)=e^{i\vec{q}\cdot\vec{r}_j}\,, \tag{1.1}$$

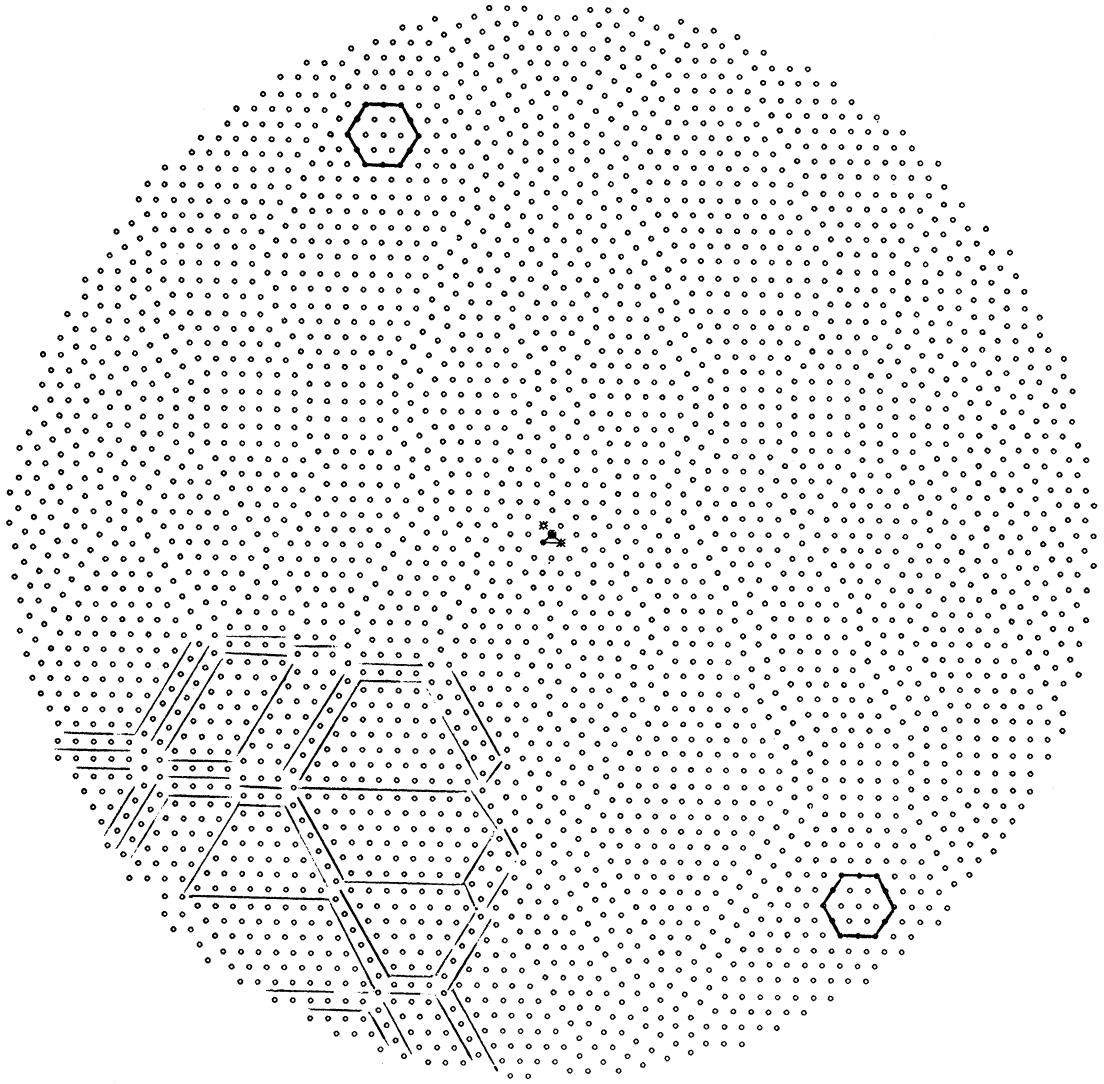

FIG. 1. Array of approximately 3200 disks deposited around a smaller one via a deterministic packing algorithm. The small disk has coordination number 4, and the two asterisks are 7-coordinated particles. All other disks have coordination number 6. The entire array is riddled with stacking faults, indicated explicitly by lines in the lower left corner. The orientations of the two widely separately hexagonal patches are identical.

can be associated with every particle coordinate $\vec{r}_j$. Density modulations at wave vector $\vec{q}$ are measured by the structure function,

$$S(\vec{q})=\frac{1}{N}\left\langle \left| \sum_{j=1}^{N} \rho_{\vec{q}}(\vec{r}_j) \right|^2 \right\rangle , \tag{1.2}$$

where the summation is over N particle positions $\{\vec{r}_j\}$. The angular brackets can represent an average over thermal fluctuations and/or some distribution of quenched-in disorder. The function $S(\vec{q})$ is, of course, measured in x-ray diffraction experiments. Correlations in the directions of local six-fold crystallographic axes are probed directly by[8]

$$G_6(\vec{r})=\langle \psi_6^*(\vec{r})\psi_6(\vec{0})\rangle , \tag{1.3}$$

where

$$\psi_6(\vec{r})=e^{6i\theta(\vec{r})} . \tag{1.4}$$

The field $\psi_6(\vec{r})$ is defined on the midpoints of lines joining near neighbor atoms as determined by, for example, the Dirichlet construction.[11] These lines make angles $\{\theta(\vec{r})\}$ with respect to some reference axis.

Crystalline states have extended translational or-

der and well-defined crystallographic axes, while amorphous, liquidlike arrays should exhibit only short-ranged translational and orientational correlations. An interesting example of an intermediate "hexatic" configuration is shown in Fig. 1. This circular array of disks was produced via a deterministic Bennett algorithm. All disks have the same diameter, except for a single disk in the triangular seed shown at the center. The diameter of this smaller disk is 0.4 times the diameter of the disks packed around it. The resulting array is dominated by regions of triangular crystal, interrupted by "stacking faults," across which crystalline regions are translated, but not rotated relative to one another. The faults run in those discrete directions, related by 120° rotations. Occasionally, these faults coalesce to form small regions of square lattice.

The translational order parameter (1.1) associated with Fig. 1 will clearly be largest when $\vec{q}=\vec{G}$, where $\vec{G}$ is a reciprocal-lattice vector of the defect-free triangular solid. The quantity $\rho_{\vec{G}}(\vec{r})$, however, will be dephased on a scale comparable to the separation between stacking faults. The translational correlation function

$$G_T(\vec{r}) \equiv \langle \rho_{\vec{G}}(\vec{r}) \rho^*_{\vec{G}}(\vec{0}) \rangle \tag{1.5}$$

presumably decays exponentially for large r,

$$G_T(\vec{r}) \sim e^{-r/\xi_T} \tag{1.6}$$

where the translational correlation length ξ_T is a typical microcrystallite size. *Orientational* order, on the other hand, is only slightly affected by the stacking faults. The *orientation* of the hexagonal cell in the lower right of Fig. 1 is virtually identical to that in the upper left, despite the intervening disorder. The orientational correlation function $G_6(\vec{r})$ is presumably large to distances exceeding the sample size. Since the range of orientational correlations ξ_6 exceeds the sample size, and it is in particular much larger than ξ_T,

$$\xi_6 \gg \xi_T \ . \tag{1.7}$$

Orientational correlation lengths of order 1 mm in the presence of translational order extending only a few hundred angstroms have in fact been observed via x-ray diffraction in the stacked hexatic[11] phase of smectic liquid crystals.[12] It should be stressed, however, that the microscopic structure in other systems with hexatic order is almost certainly quite different than that shown in Fig. 1. Crystals disordered by isolated dislocations, for example, also display extended orientational correlations.[7,8] It is worth emphasizing in addition that Fig. 1 should be distinguished from a crystal disrupted by a random network of *grain boundaries*. Both the orientational and translational correlations would decay on a scale comparable to the grain size in such systems.

In Sec. II we study orientational and translational order in binary mixtures of hard disks placed together according to a two-dimensional Bennett algorithm. On the scale of the 2000-disk samples considered, we find either crystalline, hexatic, or genuinely amorphous (liquidlike) arrays. To better understand the dependence on disk radii and composition, we first examine the effect of a single disk with "wrong" size placed in the triangular seed of a sample with otherwise uniform disk diameters. When the ratio of the diameter of the inhomogeneity disk to the diameter of the disks in the surrounding matrix is close to unity, the perturbation appears to heal at distances far from the center of the sample. For larger deviations of the diameter ratio from unity, however, first dislocations and then disclinations are trapped in the vicinity of the inhomogeneity disk. One might expect hexatic and amorphous arrays to result from dilute concentrations of the corresponding impurities. For still larger deviations of diameter ratios from unity, a single inhomogeneity produces chaotic arrays such as that shown in Fig. 1.

Strictly speaking, both translational and orientational correlations may ultimately decay to zero at any finite impurity concentration because of effects due to impurity clustering. We have estimated the resulting translational and orientational correlation lengths in the limit of dilute impurity concentrations and as the ratio of disk diameters tends toward unity. These lengths can be very large and are in fact both much larger than the sample size for the "crystalline arrays" studied here. Situations in which ξ_T is finite, but ξ_6 far exceeds the sample size, are also possible.

Hard-sphere arrays in three dimensions are often relaxed by imposing a softer potential, and then allowing the particles to move toward configurations of lower energy.[3] It would be interesting to observe the effect of such a relaxation on the two-dimensional arrays considered here. The isolated dislocations and disclinations trapped in many of our samples are topological defects, and cannot be removed by making local changes in a crystalline matrix.[14] Presumably, many of the defects found in the hard-disk arrays would remain after relaxation. Defects can annihilate each other or move to the boundary, however. The chaotic array of stacking faults shown in Fig. 1 might also disappear when allowed to relax in a softer potential.

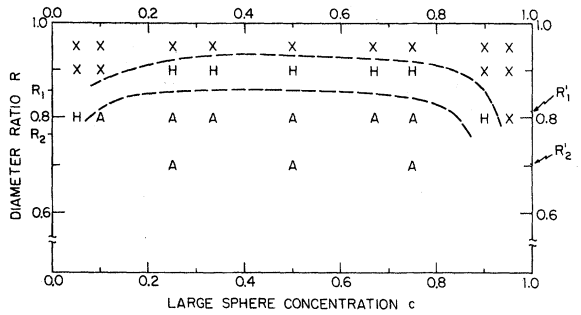

FIG. 2. Different kinds of order in binary hard-disk arrays as a function of the large-sphere concentration C and the diameter ratio R. Crystalline, hexatic, and amorphous order on the scale of our 2000-disk samples are indicated by points marked X, H, and A, respectively. These crude assignations suggest the "phase boundaries" shown as dashed lines.

Figure 1 is a good example of the "deterministic chaos" mentioned in the title of this paper. Exactly the same pattern of stacking faults would be found upon repeating the experiment.[13] In Sec. III we pursue this theme further and consider deterministic spiral growth algorithms. The most interesting results occur for an "alternating spiral," in which successive large and small disks form a curve spiraling outward from the origin. As the ratio of disk diameters is decreased from unity, we find a transition from crystalline packings to arrays, which are disordered in the angular direction of spiral growth, but translationally ordered in the radial direction. This structure is a kind of glassy analog of a rolled up two-dimensional smectic liquid crystal.

Transitions to deterministic chaos also occur in the logistic maps of the unit interval.[15] Although the systems studied here are more complex, one might hope that techniques developed for logistic maps could be profitably applied to deterministically packed hard-disk arrays. Perhaps the results presented here will stimulate further investigations along these lines.

II. TWO-DIMENSIONAL BENNETT MODEL

In this section, we discuss arrays generated via a two-dimensional Bennett algorithm.[9] The starting point is a triangular seed of hard disks. Successive disks are brought in from infinity, and placed so that they (i) just touch two disks in the growing cluster without any overlap, and (ii) are as close as possible to the centroid of the initial-seed triangle. When disks with uniform diameters are used, the result is a perfect triangular crystal. Disorder can be introduced by packing disks with two different diameters. A random number generator determines if the next disk to be packed will be large or small. The probabilities are chosen to ensure a definite composition after many steps in the procedure. Large arrays with the same composition and ratio of disk diameters seem to have statistically similar properties. The results are insensitive to which of four possible triangular seeds is used, especially in the more disordered configurations.

It is convenient to discuss the results in terms of the "phase diagram" shown in Fig. 2, as a function of the composition

$$c=\frac{N_l}{N_l+N_s} \tag{2.1}$$

and the ratio of disk diameters

$$R=d_s/d_l\ . \tag{2.2}$$

Here, N_l and N_s are the numbers of large and small disks, while d_l and d_s are the corresponding disk diameters. Since a state with parameter values (c,R) is equivalent to one defined by $(1-c,1/R)$, it suffices to consider only the ranges $0\le c\le 1$ and $0\le R\le 1$. The lines $c=0$ and $c=1$ must result in crystalline packings, as does the line $R=1$. The behavior for small R is complicated, because small disks can become lost in the spaces between the large ones. To avoid such complications, we have concentrated our attention for finite compositions on ratios such that

$$R\gtrsim 0.7\ . \tag{2.3}$$

A. Results for a single-impurity disk

In Ref. 7 hexatic configurations of ball bearings were generated by dislocations trapped on a minority concentration of large spheres. Here, we look for defects trapped by a single impurity placed in the seed which forms the starting point of the Bennett algorithm. The algorithm is essentially deterministic from this point on. In contrast to experiments on real ball bearings, it is particularly easy to vary R smoothly on the computer. In some sense, the results should be relevant for dilute concentrations of impurities with the corresponding value of R, i.e., near the lines $c=0$ and $c=1$ in Fig. 2. The isolated impurity disks discussed here, however, occupy special positions at the center of the growing cluster. Their ability to trap defects can change when packed further away from the origin.

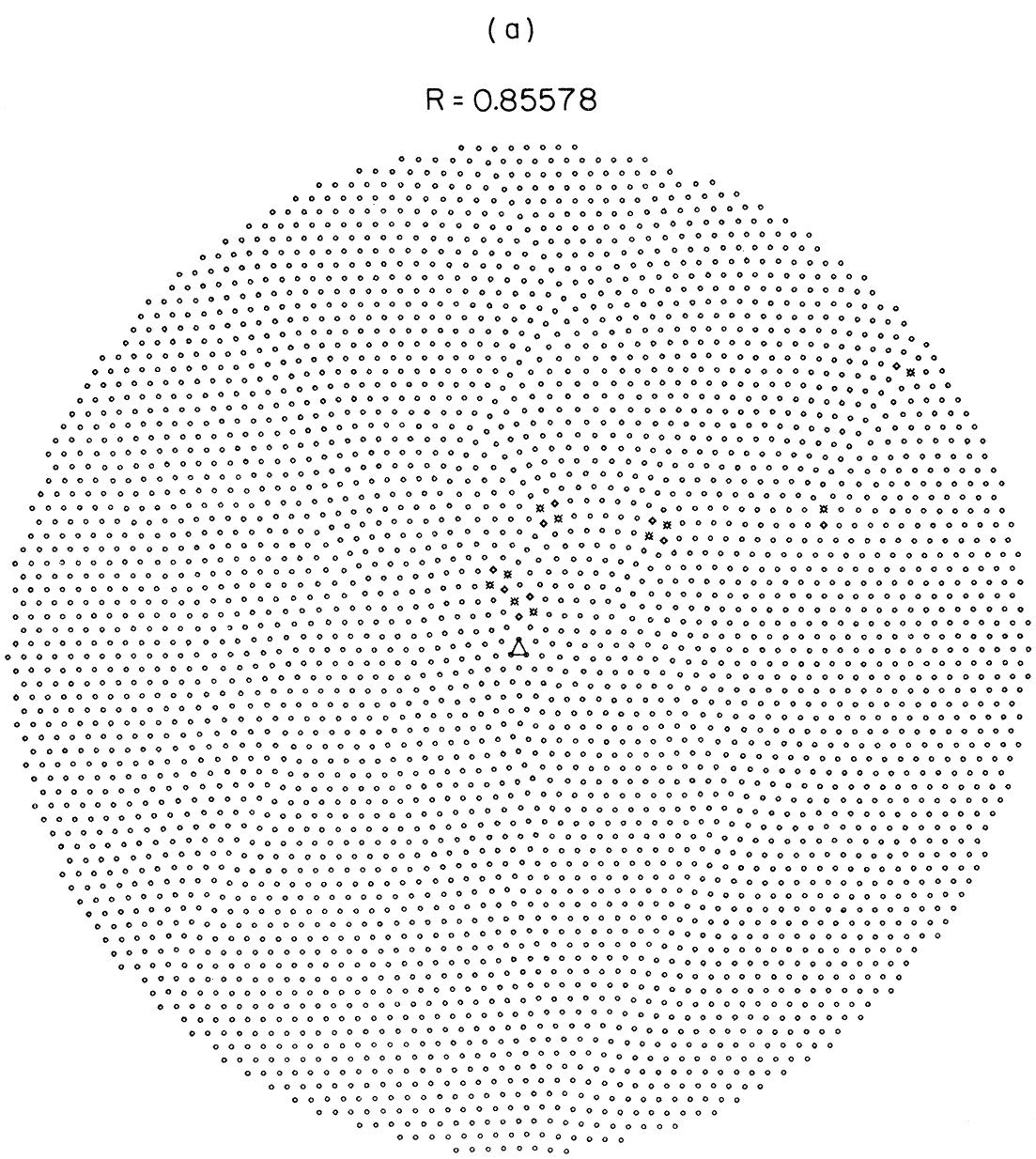

FIG. 3. Configurations of identical small disks packed around a large one at four different diameter ratios. The triangle at the center is the seed which initiates the Bennett packing algorithm. 7-coordinated particles are indicated by asterisks, and 5-coordinated ones by diamonds. The 5's and 7's may be viewed as disclinations, while isolated 5-7 pairs are dislocations. All other particles have coordination number six.

Defects are easily visualized in two dimensions via a coordination number construction used for equilibrium melting by McTague *et al.*[16] and to analyze ball-bearing arrays by Spaepen.[5] One first covers a particle configuration with a net of triangles whose vertices are at particle positions and whose sides connect near neighbors. Near neighbors are determined by the Dirichlet construction[11] or some other convenient algorithm such that no near-neighbor bonds cross. A corollary of a theorem due to Euler implies that the mean particle coordination number obtained in this way for an infinite sample is exactly six.[11] Disclinations show up as isolated 5- or 7-coordinated atoms. The deviation of the coordination number from 6 acts like a conserved topological charge. Dislocations appear

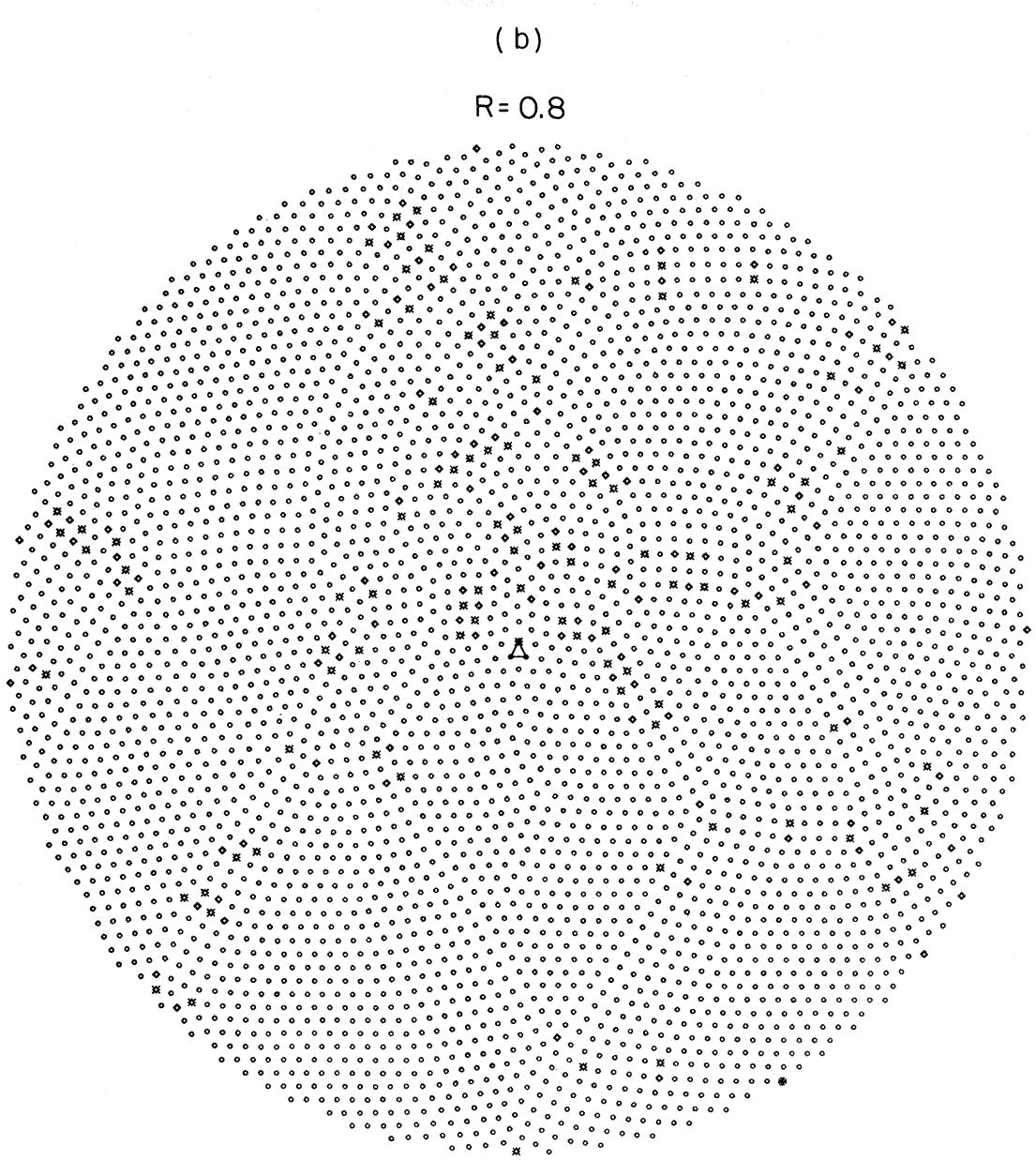

FIG. 3. (*Continued.*)

as isolated 5-7 pairs of disclinations. The corresponding Burgers vector is just the "dipole moment" of the disclination charges rotated by 90°. Grain boundaries are described by alternating -5-7-5-7- chains. This construction, although often quite illuminating, is less useful in very amorphous arrays, where the density of 5's and 7's can be quite high. It also depends sensitively on the algorithm for assigning near neighbors in regions where the particles approximate a square lattice.

As R decreases from unity with a single large disk at the center, the resulting disturbance initially heals at distances far from the center. All coordination numbers in the 4000-atom clusters we generated were 6 for $R \geq 0.871\,85$. At this value of R, two quartets of anomalous coordination numbers appear. The quartets are "charge quadrupoles," in the sense that each has two 5's and two 7's and carries no net Burgers vector. They have little effect on their surrounding environment. At $R_1 = 0.855\,78$, two isolated dislocations appear, in addition to the quartets like those described above [see Fig. 3(a)]. The two quartets at the center of Fig. 3(a) were the only anomalous coordination numbers for

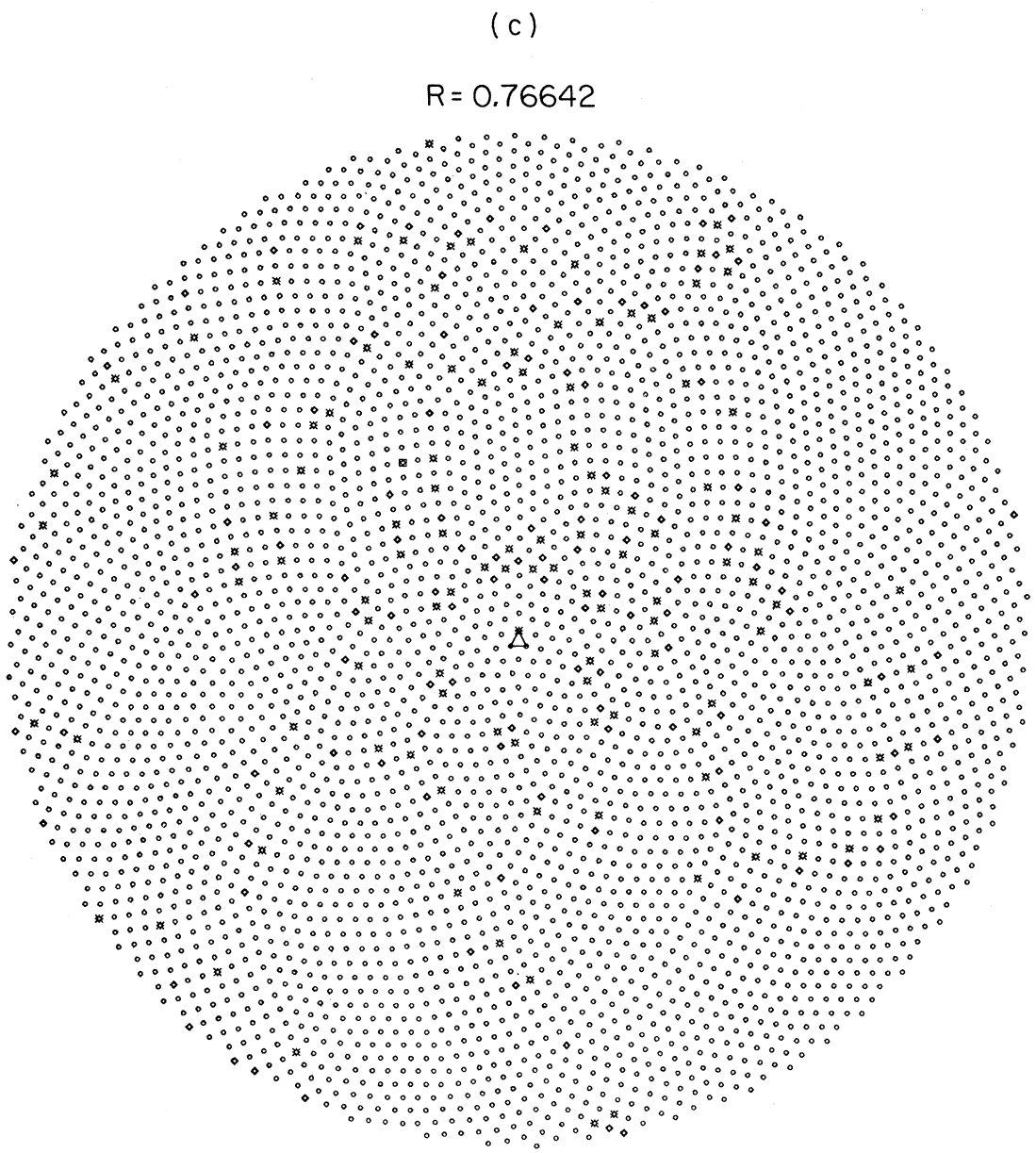

FIG. 3. (*Continued.*)

$R=0.855\,79$. The isolated dislocations occur just before the coordination of the large disk changes from 6 to 7. For smaller R values, the 7 on the impurity disk is always compensated by a nearby 5, and more dislocations appear. Some of the 5-7 dislocation dipoles begin to separate, however, as shown in Fig. 3(b) for $R=0.8$. Note that the bilateral symmetry present in the seed dies off very rapidly, in contrast to more ordered structures like Fig. 1. Presumably, this happens because Fig. 3(b) contains many more anomalous coordination numbers.

One might expect a trapped disclination when seven smaller disks just fit snugly around the inhomogeneity. The resulting array (with[17] $R=R_2\approx 0.766\,42$) is shown in Fig. 3(c). There is indeed an isolated 7 at the origin, and a scattering of widely separated 5's and 7's at distances which are quite far away. As R decreases still further, the arrays continue to exhibit swirling colineations of particles like those evident in Fig. 3(c). Disclinations with coordination numbers 7, 8, and 9 remain trapped at the origin. A qualitatively different ar-

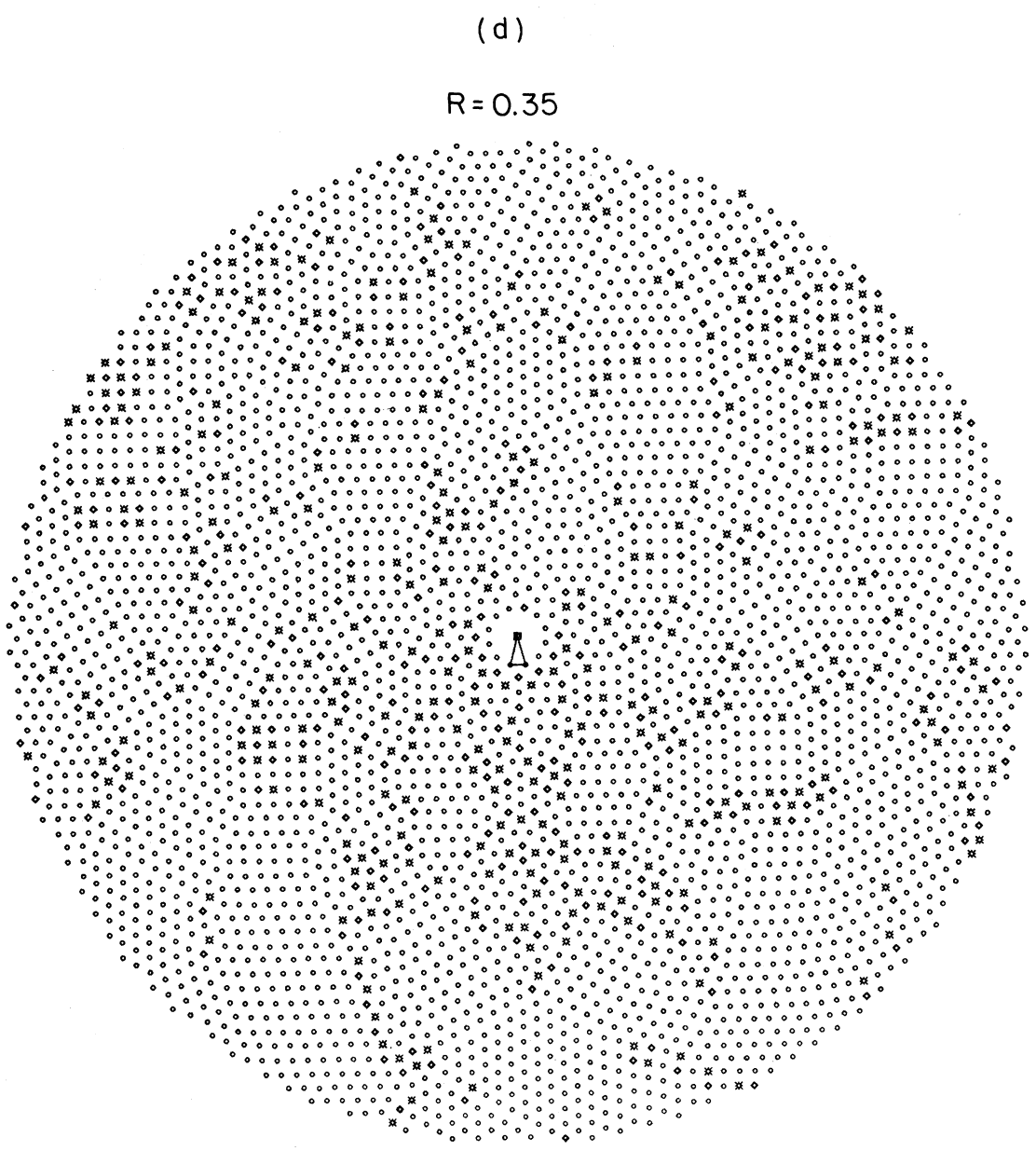

FIG. 3. (*Continued.*)

ray is obtained when R reaches 0.35 [Fig. 3(d)]. Here, the order is broken up by a few stacking faults, small portions of square lattice, and many grain boundaries. A good example of a grain boundary occurs just to the left of the bottom of the figure. The swirling pattern of Fig. 3(c) is recovered (with a 10-coordinated disclination at the origin) for $R=0.3$.

The behavior as R decreases from unity with a *small* disk at the center is also of interest. As shown in Fig. 4(a) for $R=0.9$, the perturbation due to the small disk eventually heals. At $R=0.856\,38$, two quadrapoles appear, followed by an isolated dislocation appearing at the edge of our 4000-disk samples for $R=R_1'=0.823\,70$. A quadrapole with a 5 on the inhomogeneity disk also appears at roughly this value. This dislocation moves in toward the center for $R=0.815\,77$ and $R=0.814\,79$ [Figs. 4(b) and 4(c)]. Note the additional topological debris (carrying a nonvanishing Burgers vector) in the upper-left portion of Fig. 4(c).

When $R=R_2'\approx 0.7013$, five larger disks are just

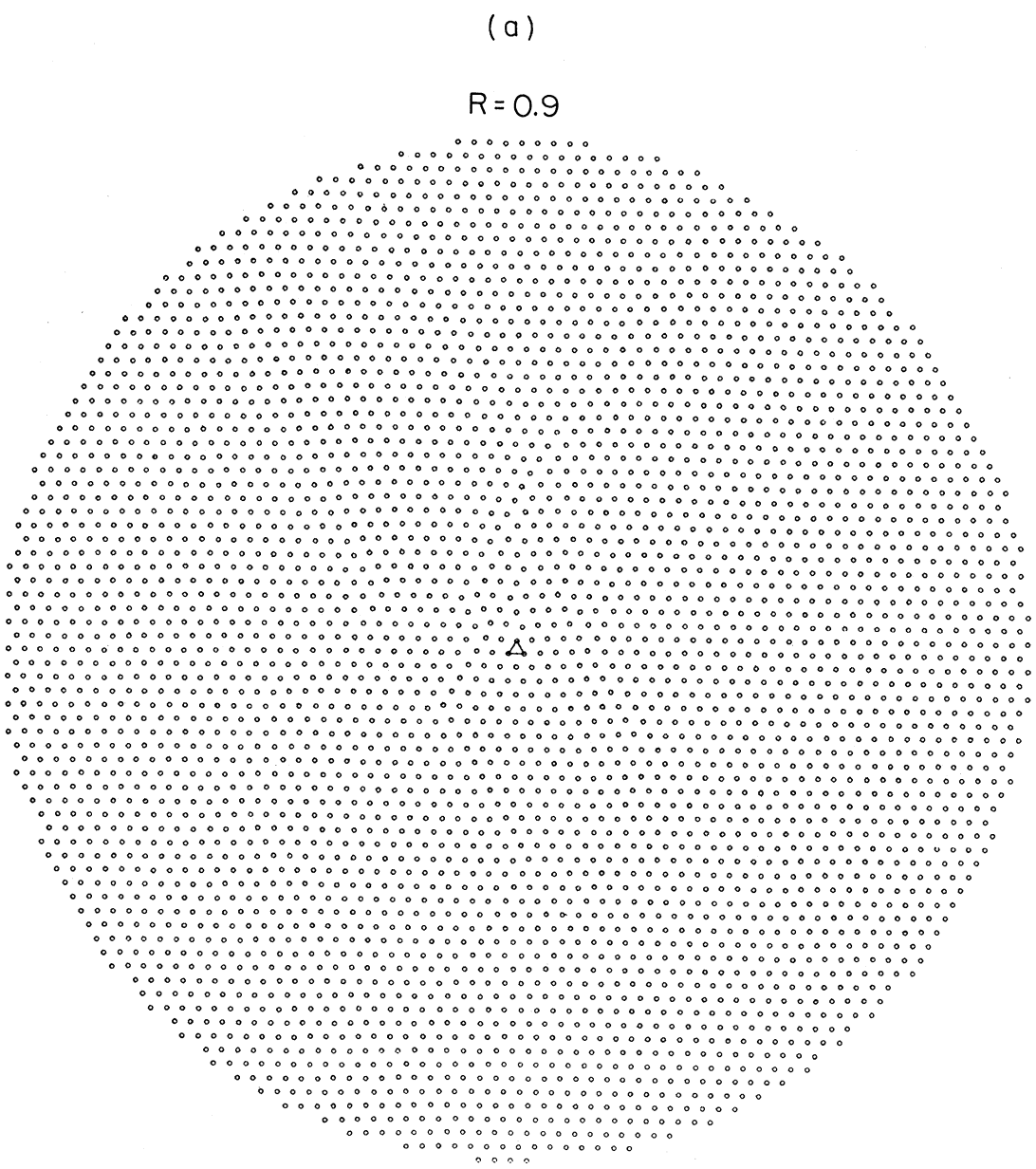

FIG. 4. Configurations of identical large disks packed around a small one at four different diameter ratios.

able to form a pentagonal configuration around the inhomogeneity. The resulting array [Fig. 4(d)] has an isolated fivefold disclination at the origin, and other isolated 5's and 7's as well. Although a wedge of defect-free material appears below the seed, we expect that this grain will eventually be choked off. Defects are already beginning to appear near the bottom. As R decreases further, the arrays eventually organize into an arrangement of stacking faults like that shown in Fig. 1 and discussed in Sec. I. These curious configurations occur for a range of diameter ratios near $R=0.40$.

The configurations triggered by a small impurity disk at the origin should be contrasted with those found in quenched ball-bearing arrays.[7] Here, isolated small spheres are usually found imprisoned in a rigid hexagonal hole formed by the matrix of larger spheres. Once trapped, a small impurity sphere is powerless to impede formation of a crystalline array. The behavior for a *large* inhomo-

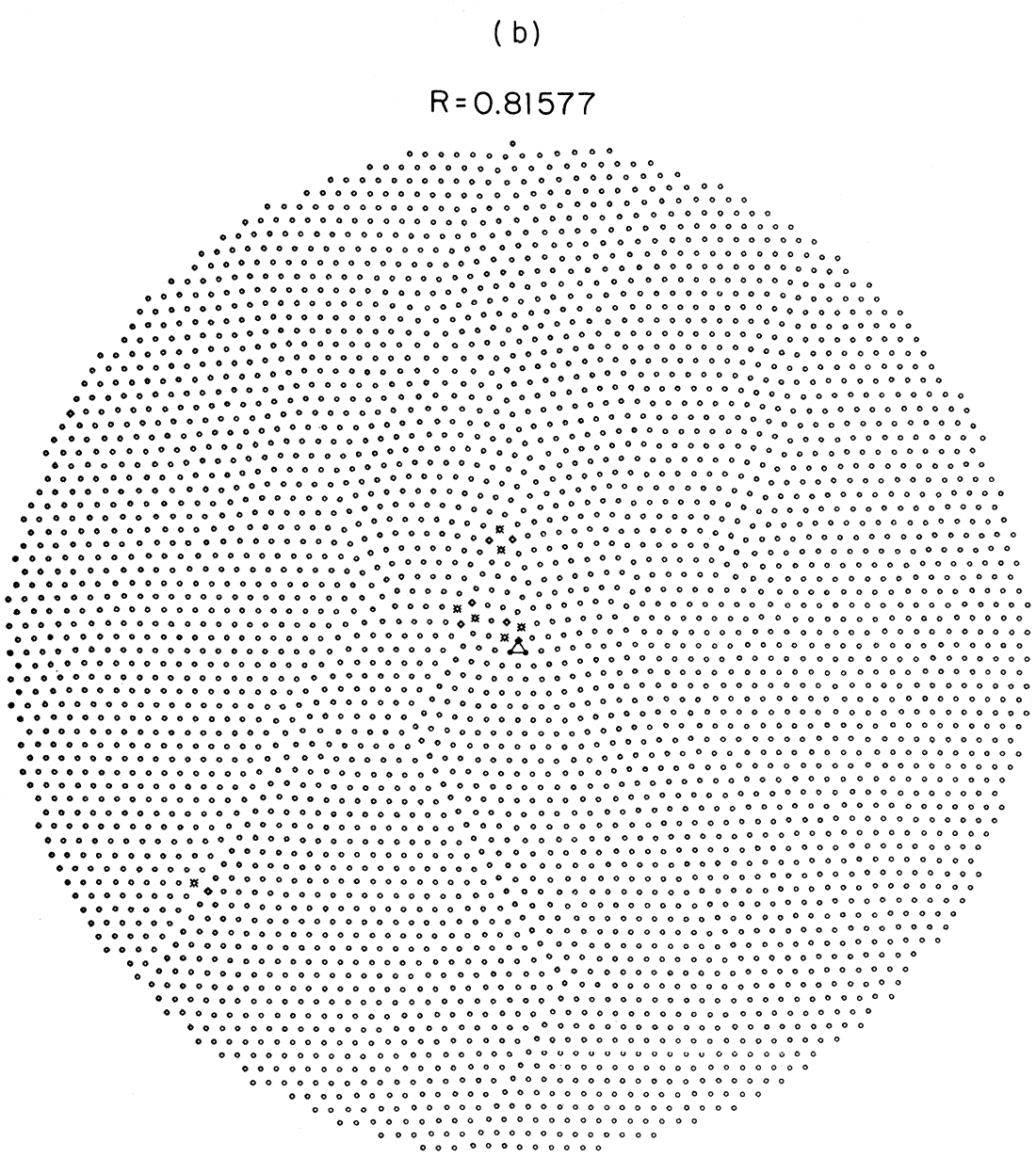

FIG. 4. (*Continued.*)

geneity disk is qualitatively similar to the ball-bearing results, at least for $R \gtrsim 0.8$. It is conceivable, however, that the disclination trapped by the impurity in Fig. 3(c) would screen itself at least partially by polarizing the surrounding medium in an annealed ball-bearing array. It would be interesting to see how the effect of a single impurity disk is altered by annealing or by softening the potential.

B. Binary mixtures

Figure 5(a) shows a 50-50 mixture of 2000 hard disks with diameter ratio $R=0.80$ generated via the Bennett algorithm. The structure function $S(\vec{q})$ is shown in Fig. 5(b). The high, approximately uniform density of 5- and 7-coordinated particles, and the isotropy of $S(\vec{q})$ indicate an amorphous, liquid-

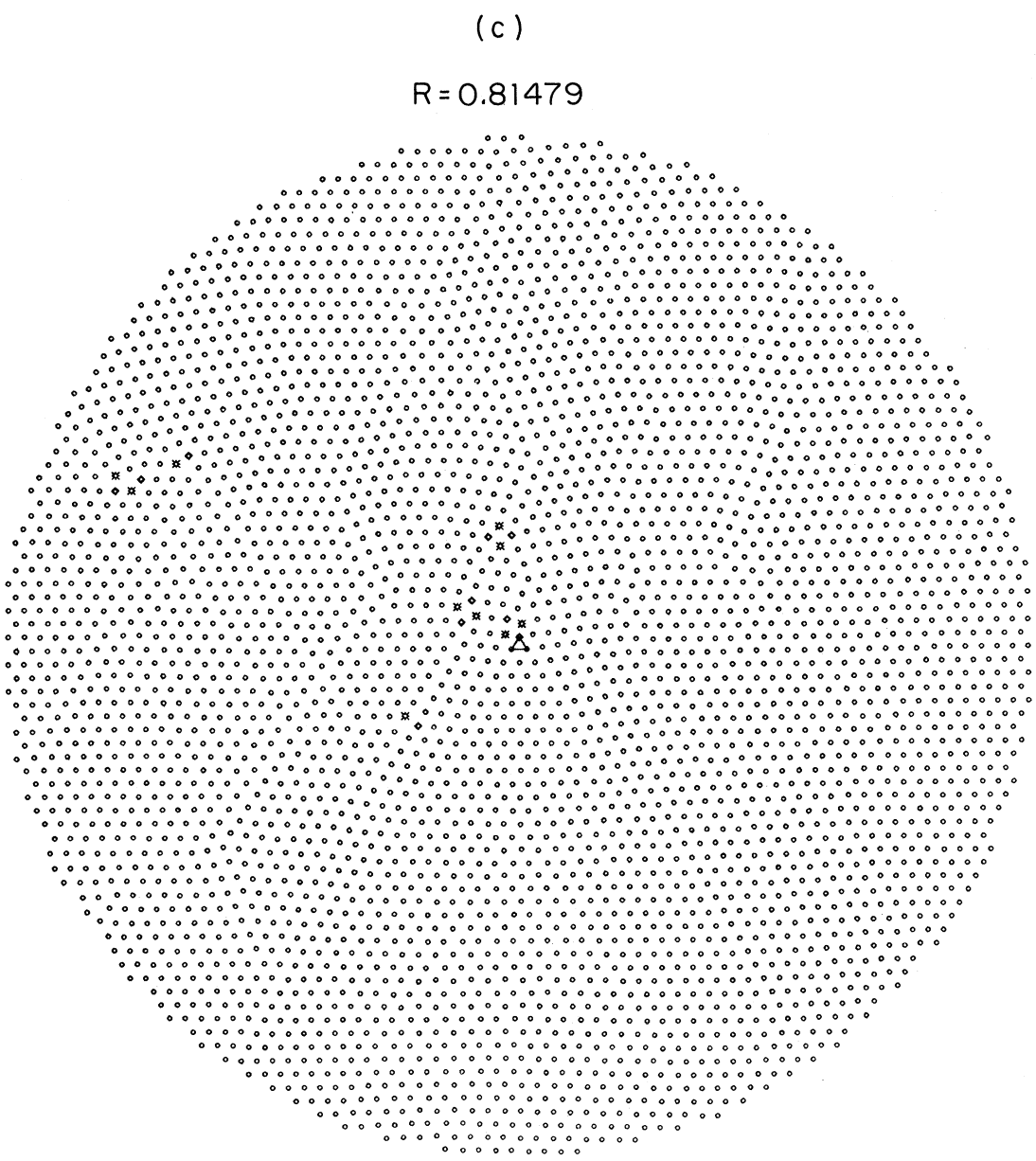

FIG. 4. (*Continued.*)

like configuration. The structure function, as well as the orientational correlation function $G_6(\vec{r})$ [Fig. 5(c)] were obtained via a fast-Fourier-transform technique from an approximately 1200-particle square section cut out of the center of the circular sample. The seed was composed of two small disks and one large one. The functions $S(\vec{q})$ and $G_6(\vec{r})$ did not change significantly from run to run, or when the seed was changed to one small and two large disks.

Figure 6 shows the average "packing fraction" of disks as a function of sample radius for the two seeds mentioned above. Qualitatively similar results were obtained for other compositions and diameter ratios. These packing fractions were obtained by determining the area covered by all disks (large and small) contained in a circle of radius r inscribed about the centroid of the seed triangle and dividing by πr^2. Although there is considerable scatter, the results for both seeds seem to be tending toward a

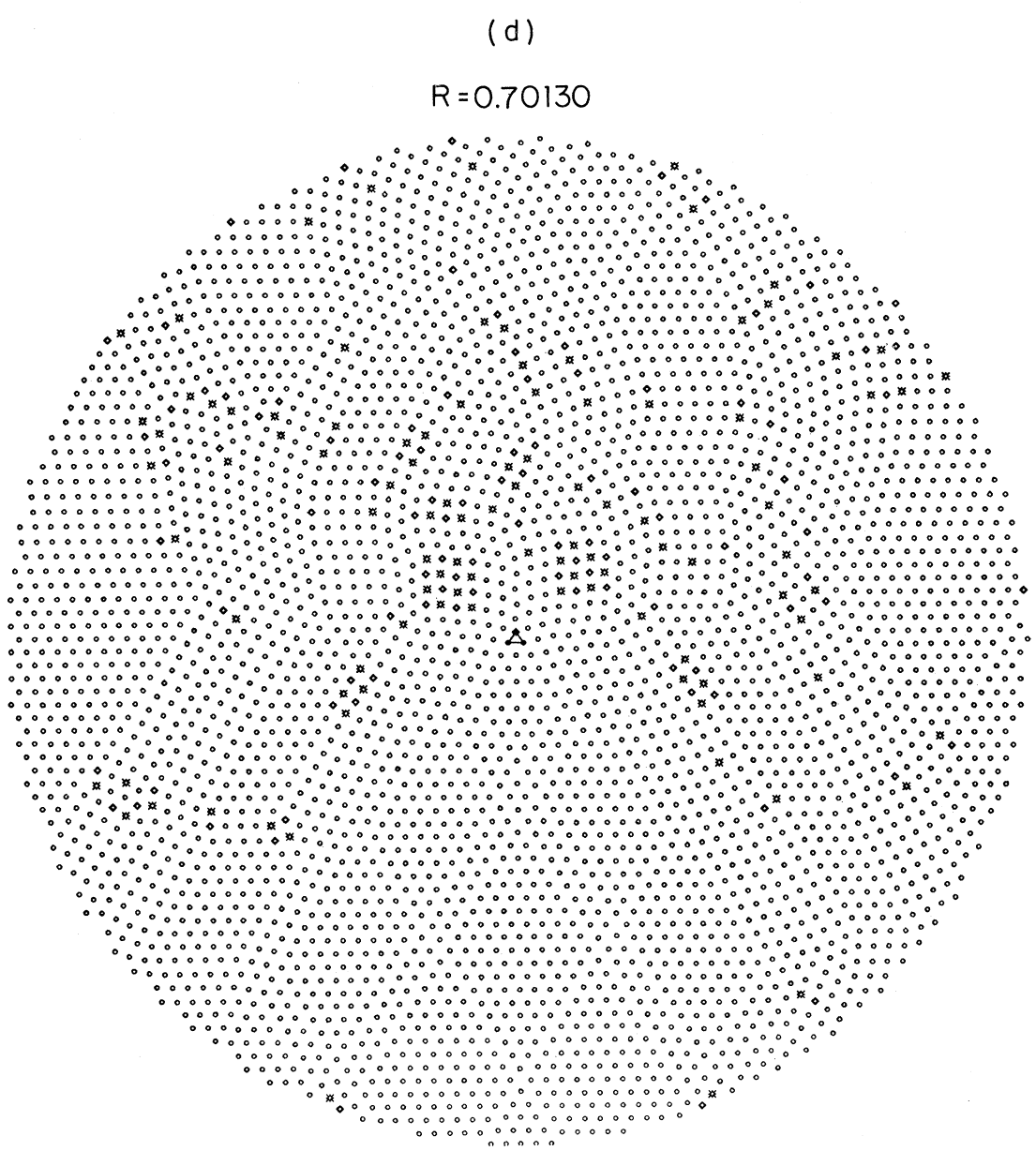

FIG. 4. (*Continued.*)

limiting amorphous packing fraction

$$\rho_A \approx 0.825 \pm 0.02 \ . \tag{2.4}$$

The packing fraction of a "phase-separated" configuration consisting of two perfect triangular lattices each containing equal numbers of large or small disks is

$$\rho^* = \frac{\pi}{2\sqrt{3}} = 0.907 > \rho_A \ . \tag{2.5}$$

From the width of the first ring in $S(\vec{q})$ [Fig. 5(b)], we can infer that translational correlations persist for at most two or three mean disk diameters. The isotropy of this pattern reveals the absence of extended orientational correlations. Figure 5(c) shows that in fact $G_6(\vec{r})$ drops to zero within a few mean disk diameters.

A considerably more ordered array is generated for 50-50 mixtures with $R=0.95$ (Fig. 7). There are a few trapped dislocation pairs, and six symmetrical Bragg spots are evident in the structure function. The orientational correlation function decays to a large nonzero value for large r. As noted in Ref. 7, quenched-in volume fluctuations caused by the in-

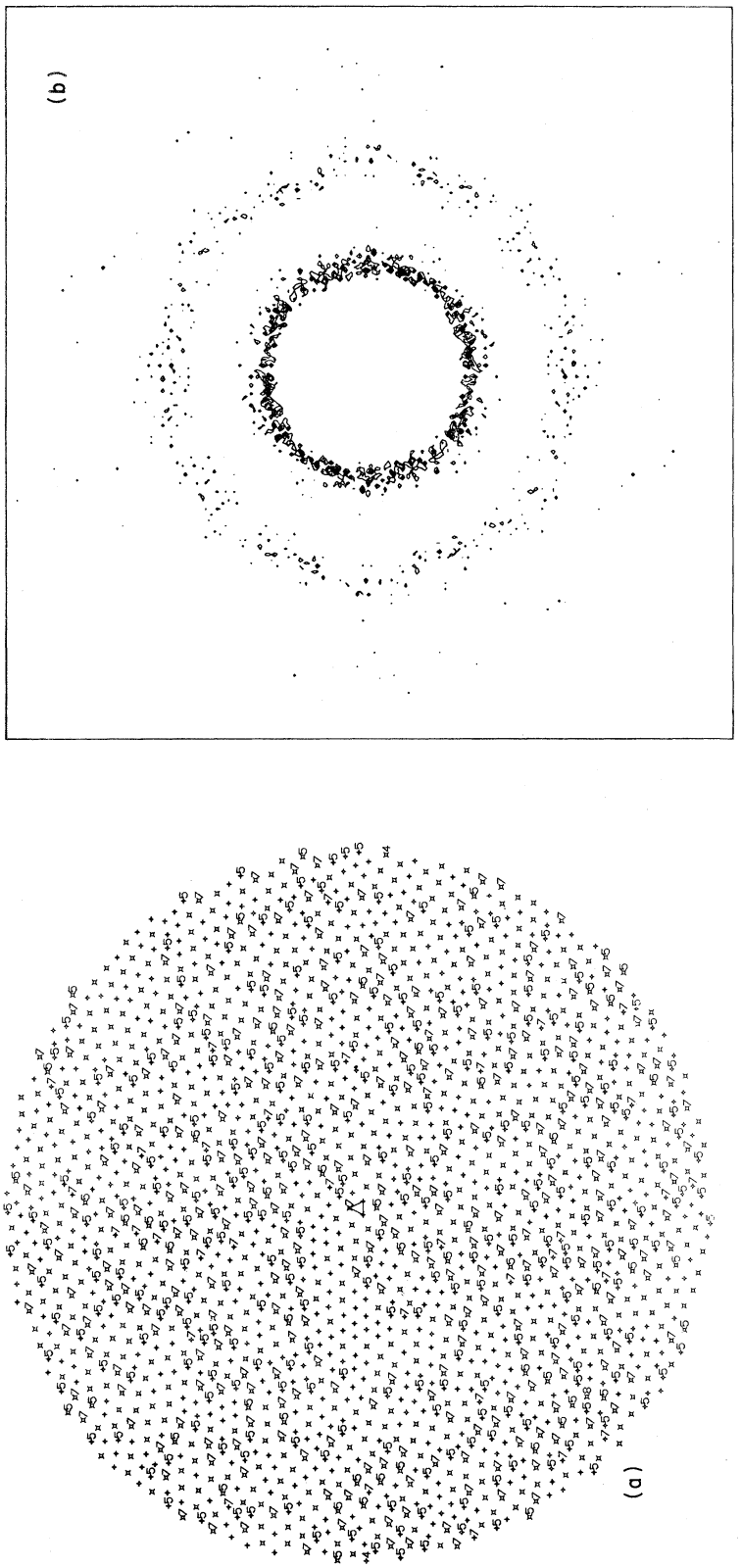

FIG. 5. (a) Array of 1010 small disks and 990 large ones with the ratio of diameters $R=0.8$. Small disks are plotted as crosses, large ones are plotted as squares. Coordination numbers deviating from 6 are indicated explicitly. (b) Structure factor $S(\vec{q})$ calculated from a square sample of 611 small disks and 598 large ones cut from the center of the system plotted in (a). The isotropic contours of intensity indicate a translationally and orientationally disordered "amorphous" sample. (c) Orientational correlation function $G_6(\vec{r})$.

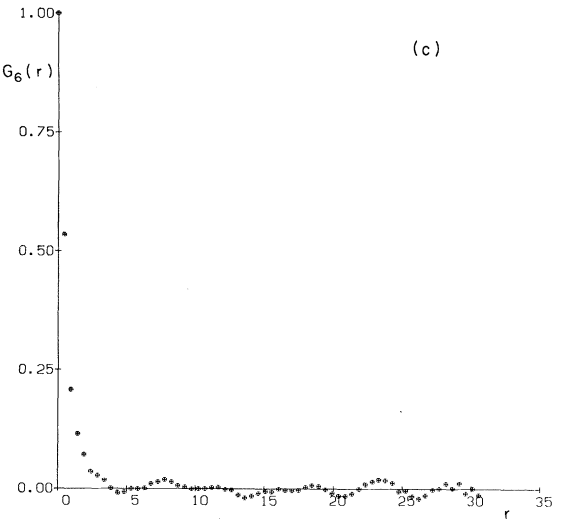

FIG. 5. (*Continued.*)

homogeneous disk diameters in elastic solids lead to *power-law* singularities at a set of reciprocal-lattice vectors $\{\vec{G}\}$,

$$S(\vec{q}) \sim \frac{1}{|\vec{q}-\vec{G}|^{2-\eta_{\vec{G}}}} . \tag{2.6}$$

The system is structurally like a solid at a finite temperature with no disorder. The exponent $\eta_{\vec{G}}$ depends on the amount of frozen-in disorder. Although Fig. 7(b) is certainly consistent with Eq. (2.6), it is not clear to what extent our deterministically packed hard-disk arrays are describable by an *elastic* solid with quenched disorder.

Figure 8 shows a 50-50 mixture of disks with $R=0.90$. The numerous dislocations (5-7 pairs) evident in Fig. 8(b) are often well separated, but occasionally seem to align into grain boundaries. Translational correlations extending roughly four or five mean disk diameters are suggested by the radial width of $S(\vec{q})$. There is, however, a noticeable sixfold anisotropy in the first ring. The correlation $G_6(\vec{r})$, after a rapid drop, decays very slowly. The large-r behavior of $G_6(r)$ is consistent with the *algebraic* decay of orientational order expected in arrays disordered primarily by quenched-in dislocations.[7] The structural properties of this configuration are quite similar to the equilibrium hexatic phase.[6] The hydrodynamic theory of hexatics[6] also suggests a tendency for dislocations to align in grain boundaries. The orientational correlations in Fig. 8(c) appear qualitatively different from those characteristic of amorphous [Fig. 5(c)] and crystalline [Fig. 7(c)] arrays.

We now survey results for arrays generated at a number of different composition and diameter ratios in the ranges $0.05 \leq c \leq 0.95$, $R \geq 0.7$. The resulting structure and orientational correlation functions were classed as amorphous, crystalline, or hexatic, depending on whether they most resembled Figs. 5, 7, or 8. These crude assignations are summarized in Fig. 2. At least on the scale of our 2000 particle samples, one finds regions which are amorphous, crystalline, or hexatic. Although it is hard to draw precise conclusions, areas of hexatic behavior seem interposed between crystalline and amorphous regions.

It is tempting to introduce the "phase boundaries" indicated by dashed lines in Fig. 2. The precise meaning of such boundaries, however, is unclear. One might worry about the effect of the seed configuration on our finite size samples. Changing the seed did occasionally lead to noticeable changes in $S(\vec{q})$ and $G_6(\vec{r})$, particularly in the more ordered samples. It is also possible that, strictly speaking, all configurations with the slightest amount of disorder will be amorphous, in the sense of having finite (although perhaps very large) translational and orientational correlation lengths. Although isolated impurities may perturb the order only slightly, relatively improbable *clusters* of inhomogeneous disks could conspire to trap dislocations and disclinations. Translational and orientational coherence

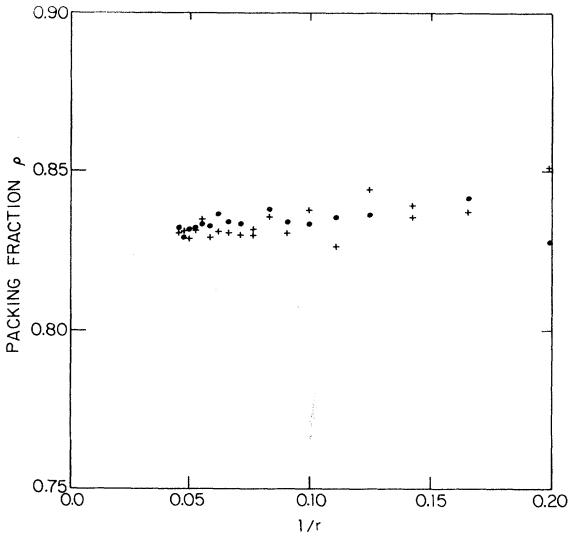

FIG. 6. Packing fraction for disks contained within circles of radius r as a function of r^{-1} in two samples at 50-50 concentration with $R=0.8$. The samples were obtained from different starting seeds and realizations of the Bennett algorithm.

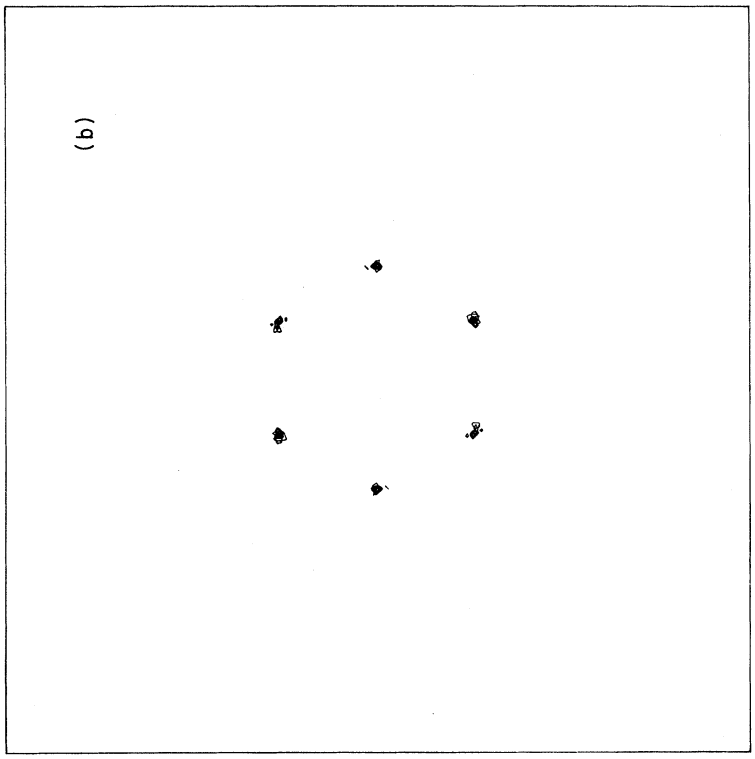

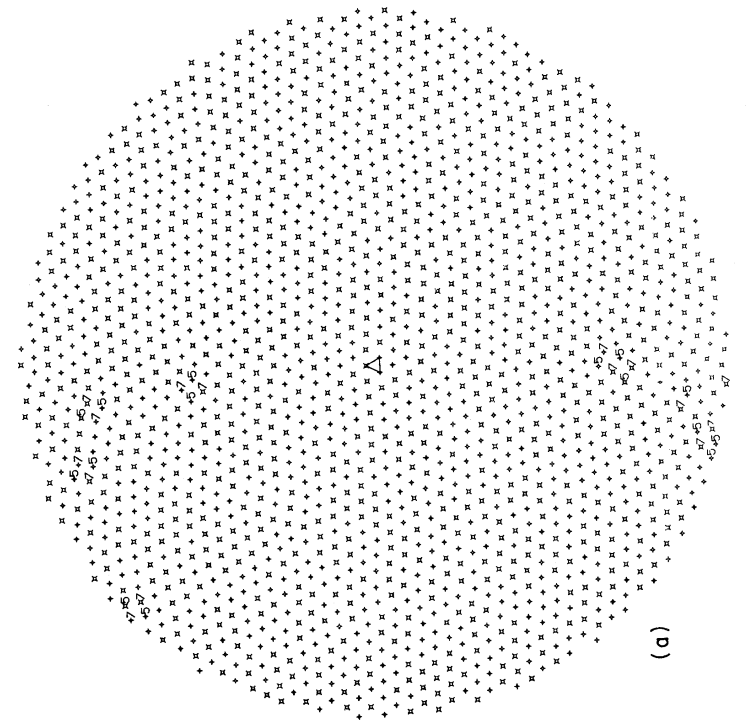

FIG. 7 (a) Array of 1010 small disks and 990 larger ones with the ratio of diameters $R=0.95$. There are only a few topological defects and the system looks crystalline. (b) Relatively sharp peaks of the structure factor $S(\vec{q})$ for a subset of 690 small and 690 large disks, extracted from the sample in (a). (c) Orientational correlation function $G_6(\vec{r})$ for sample described in (b).

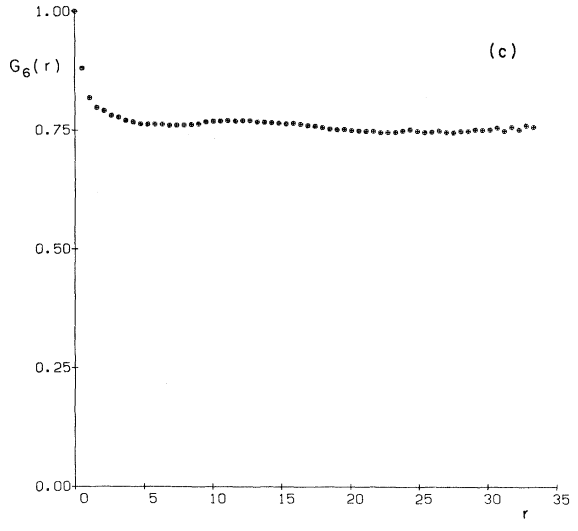

FIG. 7. (*Continued.*)

would then be destroyed on scales comparable to the separation between these clusters.

Assuming the above picture is correct, these lengths can be estimated for low-impurity concentrations and for R near 1. For concreteness, we discuss dilute concentrations of large disks, and assume that such disks trap isolated dislocations for $R<R_1$, and isolated disclinations for $R<R_2<R_1$. This scenario is consistent with our results for a single large disk at the origin. When R is less than R_2, all samples will be amorphous when viewed on a large enough scale, since the trapped disclinations break up both translational and orientational order. For $R_2<R<R_1$, translational order will be destroyed by dislocations trapped on the large disks. However, order can also be broken up at sufficiently large scales, for any R, provided *clusters* of impurities can trap dislocations and disclinations.

To estimate this effect, let us take $R \lesssim 1$, and consider the effect of a roughly circular cluster of n neighboring impurities, with $n \gg 1$. These unusual configurations occur with a number density per unit area of roughly

$$\rho_i(n) \sim c^n / d_s^2 , \tag{2.7}$$

where c is the concentration of large disks. The diameter of the cluster is of order $\sqrt{n}\, d_l$. When embedded in a matrix of smaller disks, we suppose that its effect on distant regions is like a *single* impurity disk at the center, with an effective diameter $\tilde{d} > d_l$. Replacing the original cluster by $n-1$ small disks and one larger one, we see that $\tilde{d}$ must satisfy

$$\tilde{d}^2 + (n-1)d_s^2 \approx n d_l^2 , \tag{2.8}$$

so that the new cluster occupies the same area as the original one. In the limits $n \gg 1$ and $R \to 1$, we find that the new effective diameter ratio is

$$\tilde{R} \equiv \frac{d_s}{\tilde{d}} \approx [2n(1-R)+1]^{-1/2} . \tag{2.9}$$

The cluster sizes n_1 and n_2, such that dislocations and disclinations are trapped follow from equating $\tilde{R}$ to R_1 and R_2, are

$$n_1 = \frac{1-R_1^2}{2R_1^2} \frac{1}{(1-R)} \tag{2.10a}$$

for dislocation trapping, and

$$n_2 = \frac{1-R_2^2}{2R_2^2} \frac{1}{(1-R)} \tag{2.10b}$$

for disclination trapping. Upon inserting these results into Eq. (2.7), we can define translational and orientational correlation lengths as the separation between the corresponding clusters,

$$\xi_T \equiv 1/\sqrt{\rho_i(n_1)} , \tag{2.11a}$$

$$\xi_6 \equiv 1/\sqrt{\rho_i(n_2)} . \tag{2.11b}$$

As c tends to zero, these lengths diverge algebraically,

$$\xi_T \sim d_s / c^{(1/2)n_1} , \tag{2.12a}$$

$$\xi_6 \sim d_s / c^{(1/2)n_2} . \tag{2.12b}$$

Note from Eq. (2.10) that exponents can be quite large for $R \lesssim 1$. As R tends towards unity for fixed $c > 0$, we find a rapid exponential divergence,

$$\xi_T \sim d_s \exp\left[\left[\frac{(1-R_1^2)\,|\ln c\,|}{4R_1^2} \right] \Big/ (1-R) \right] , \tag{2.13a}$$

$$\xi_6 \sim d_s \exp\left[\left[\frac{(1-R_2^2)\,|\ln c\,|}{4R_2^2} \right] \Big/ (1-R) \right] . \tag{2.13b}$$

Note that since $R_1 > R_2$, ξ_6 always exceeds ξ_T. In fact, the ratio ξ_6/ξ_T diverges as $c \to 0$ or $R \to 1$. As c tends to zero for $R_1 < R < R_2$, ξ_T should behave as in Eq. (2.12a) with $n_1 \sim 1$. Since n_2 is of order three or four times n_2 in this range of R, ξ_6 will again be much larger than ξ_T. Finite size samples will appear hexatic, just as one would have

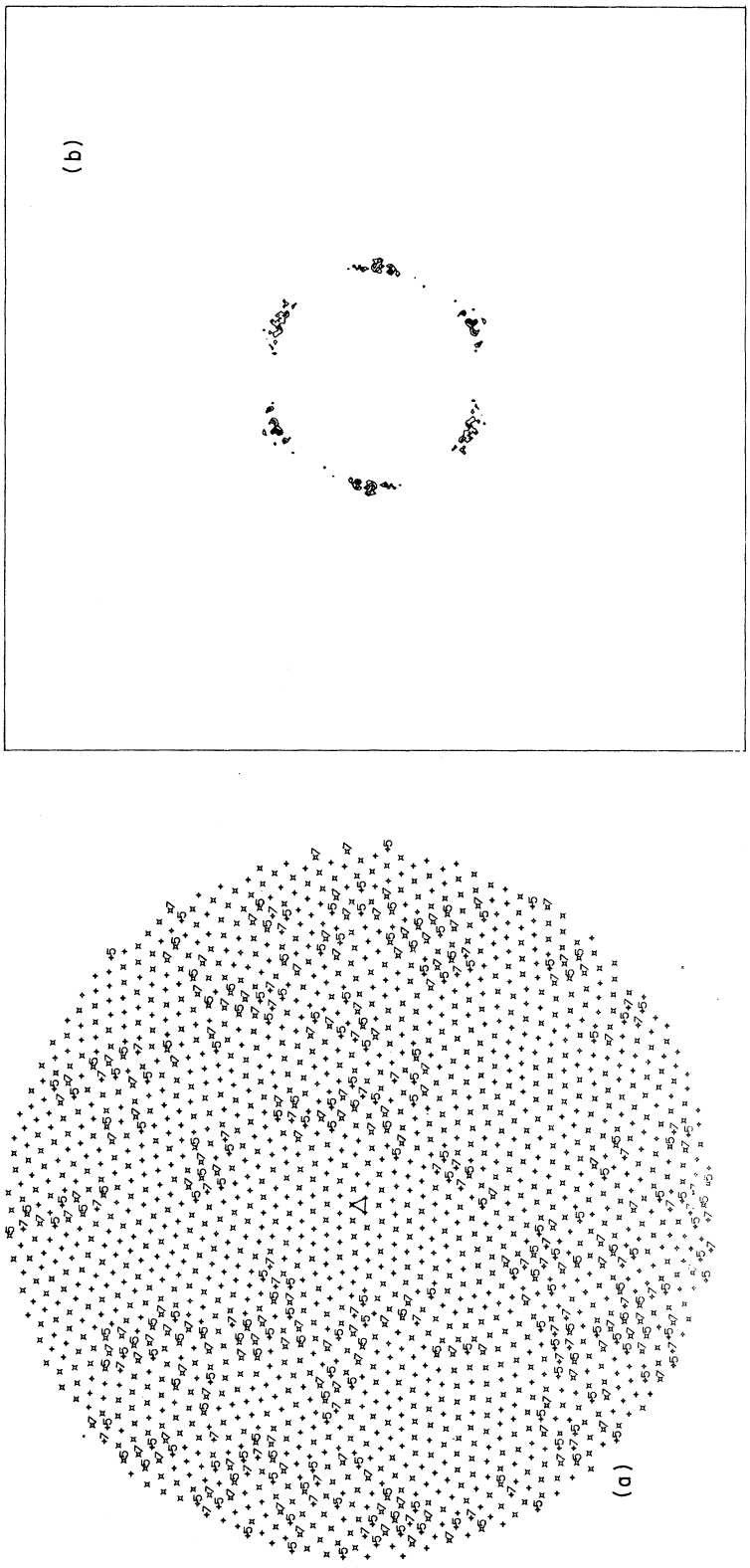

FIG. 8. (a) Sample of 990 small disks and 1010 large ones at the ratio of diameter $R=0.9$. The degree of order is intermediate between that shown in Figs. 5 and 7. (b) Structure factor $S(\vec{q})$ calculated from a sample of 612 small disks and 647 large ones extracted from the center of (a). (c) Orientational correlation function $G_6(r)$ for the same described as in (b).

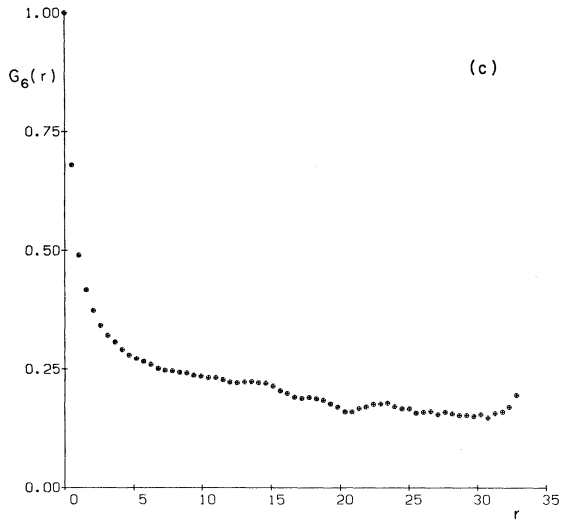

FIG. 8. (*Continued.*)

predicted ignoring the effect of impurity clusters. The lengths ξ_T and ξ_6 can be very large in the "crystalline" region of Fig. 2. Taking $R=0.95$, $c=0.05$, and assuming $R_1=0.86$, $R_2=0.77$, we find

$$\xi_T \approx 2\times 10^2 d_s, \quad \xi_6 \approx 3\times 10^4 d_s \ , \tag{2.14}$$

which are much larger than the dimensions of our sample.

Trapping of defects by impurity clusters may be of little practical importance in finite size samples, at least for small concentrations of impurities and diameter ratios near 1. One can always define approximate solid-hexatic and hexatic-liquid phase boundaries by first measuring $\xi_T(c,R)$ and $\xi_6(c,R)$. The phase boundaries appropriate to a sample of size L can then be defined by

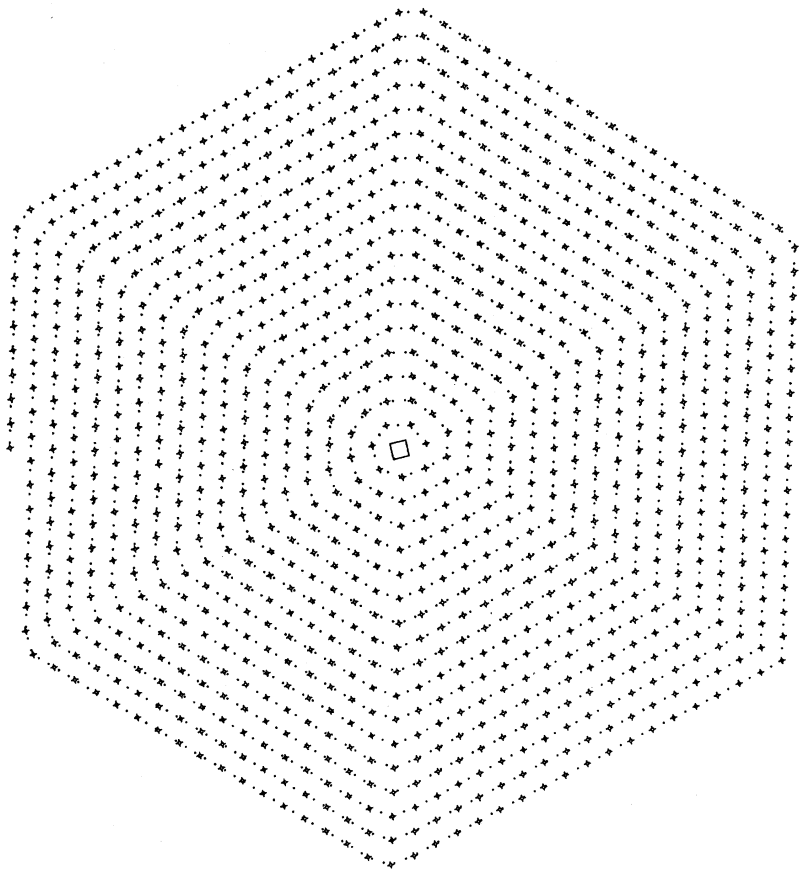

FIG. 9. Small disks (crosses) packed in a deterministic spiral around a large disk (indicated by the square) with a diameter 1.25 times larger. The small dots indicate the sequence in which the disks were deposited.

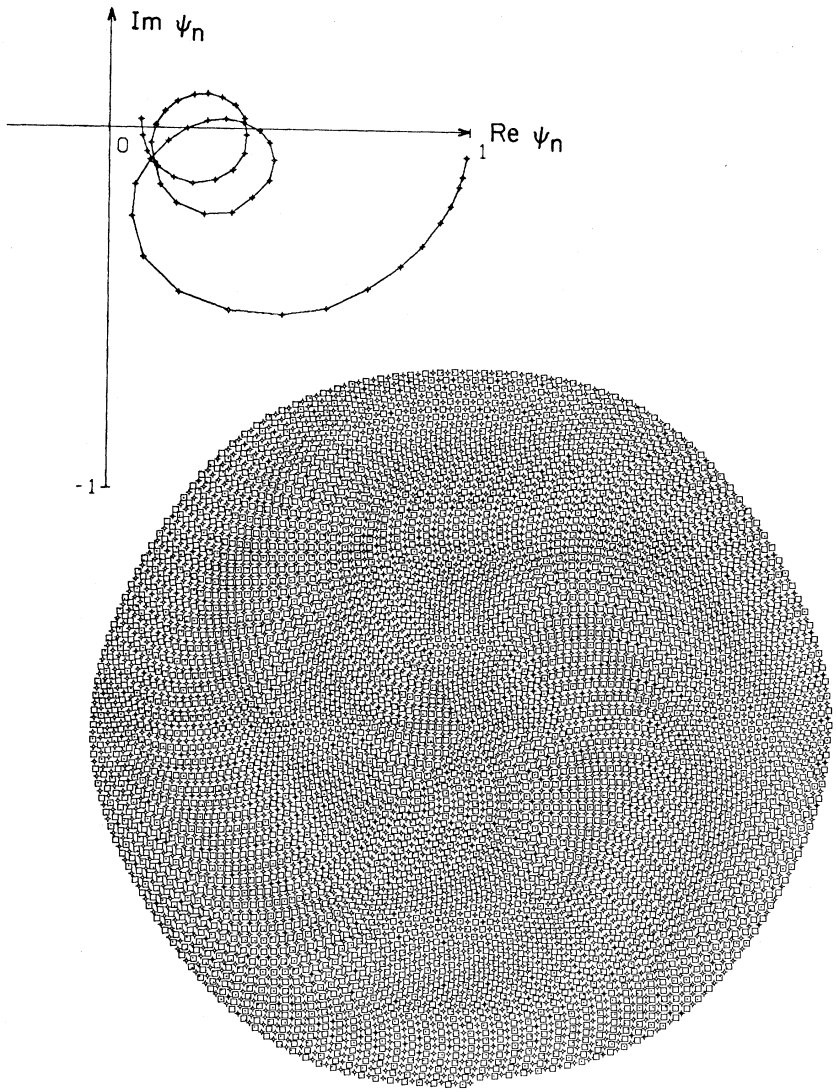

FIG. 10. "Alternating spiral" packing of 4000 small (circles) and 4000 large (squares) disks with diameter ratio $R=0.98$. Inset shows the bond orientational order parameter $\psi=e^{6i\theta}$ averaged over successive turns of the spiral.

$$\xi_T(c,R)=L \quad \text{(solid-hexatic)}\,, \tag{2.15a}$$

$$\xi_6(c,R)=L \quad \text{(hexatic-liquid)}\,. \tag{2.15b}$$

The dashed lines in Fig. 2 may be viewed as arising from these conditions, with $L\approx\sqrt{2000}\,\bar{d}$, when $\bar{d}$ is a mean disk diameter.

III. SPIRAL GROWTH ALGORITHMS

Results different from those obtained via Bennett's procedure follow from more ordered spiral growth algorithms. Starting with a single disk at the origin, more disks are added to produce a circular pattern spiraling outward from the origin (see Fig. 9). Each new disk is required to touch the previous one, as well as an additional disk in the preceding turn of the spiral. Every turn of the spiral serves as a kind of template for the next. When disks with uniform diameters are used, one grows a perfect triangular crystal. With a single disk with the "wrong" diameter at the center, the algorithm, of course, remains completely deterministic. Ambiguities present in the early stages of Bennett's construction[13] are avoided entirely. With the ratio of disk diameters as a control parameter, it

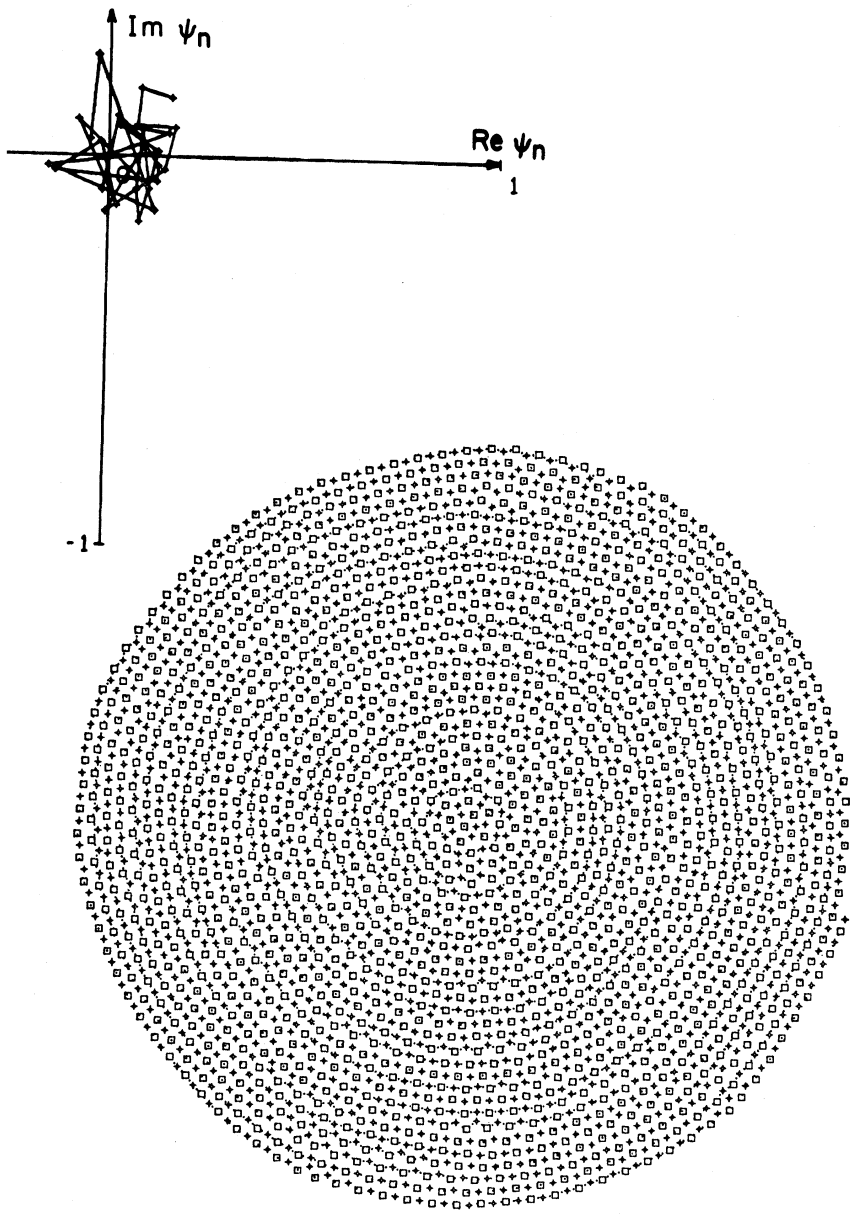

FIG. 11. Alternating spiral packing similar to Fig. 10, with 1500 large and 1500 small disks and $R=0.6$.

is interesting to search for the kind of "deterministic chaos" evident in Fig. 1.

There is actually very little "chaos" evident in Fig. 9, where the spiral is built around a large disk such that

$$\frac{d_l}{d_s}=1.25\ . \tag{3.1}$$

The second, smaller disk was placed just to the right of the large one, and the packing continued in a counterclockwise direction. Six stacking faults radiate out from the center of an otherwise perfect crystal. As d_l/d_s varies, the stacking faults disappear and reappear, and the entire pattern seems to rotate smoothly. Similar results were obtained with a single, small inhomogeneity disk at the center.

An interesting transition to deterministic chaos does occur for an "alternating spiral" algorithm. Here, one forms a spiral composed of alternating large and small disks. For diameter ratios $R\equiv d_s/d_l$ near unity, the kind of "twisted crystal"

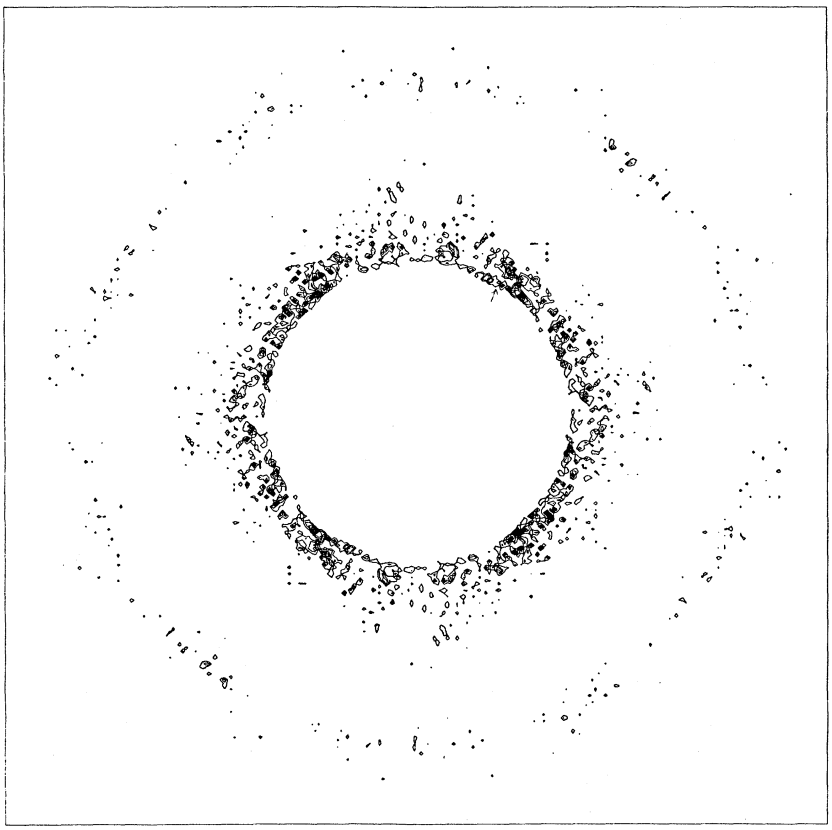

FIG. 12. Contours of constant intensity for the structure function associated with Fig. 11.

shown in Fig. 10 for $R=0.98$ is formed. The inset shows the quantity

$$\psi_n = \langle e^{6i\theta(\vec{r})} \rangle_n \ , \tag{3.2}$$

where the average is over all azimuthal near-neighbor bonds in the nth turn of the spiral. In the perfect crystal formed for $R=1$, ψ_n is fixed at unity for all n. For $R=0.98$ there is a helical variation of ψ_n with n in the complex ψ plane.

The average ψ_n becomes an increasingly erratic function of n as R is decreased further. The packing of disks found for $R=0.6$ is shown in Fig. 11. Although ψ_n is quite chaotic, a remarkable degree of residual order is evident in the x-ray structure function displayed in Fig. 12; note the sharp onset of intensity as q increases outward from the origin. The weak fourfold asymmetry is due to the square sample cut from the center of Fig. 11. This striking intensity pattern (which resembles a solar eclipse) is consistent with a periodic solidlike packing in the radial direction, but liquidlike or amorphous order azimuthally. In this sense, Fig. 11 is structurally identical to a rolled up two-dimensional smectic liquid crystal.

ACKNOWLEDGMENTS

It is a pleasure to thank P. C. Martin and B. Shraiman for many helpful conversations. We are indebted to J. Toner for discussions on the effect of impurity clustering. This research was supported by the National Science Foundation, in part through the Harvard Materials Research Laboratory, and also through Grants No. DMR 77-10210 and No. DMR82-07431. One of us (D.R.N.) would like to acknowledge a grant from the Alfred P. Sloan Foundation.

[1]J. D. Bernal, Proc. R. Soc. London, Ser. A 280, 299 (1964).
[2]C. S. Cargill, Ann. N.Y. Acad. Sci. 279, 208 (1976).
[3]M. R. Hoare, J. Non-Cryst. Solids 31, 157 (1978).
[4]P. Chaudhari and D. Turnbull, Science 199, 11 (1978).
[5]See, e.g., F. Spaepen, J. Non-Cryst. Solids 31, 207 (1978).
[6]A. S. Nowick and S. R. Mader, IBM J. Res. Dev. 1965, 358.
[7]D. R. Nelson, M. Rubinstein, and F. Spaepen, Philos. Mag. A 46, 105 (1982).
[8]B. I. Halperin and D. R. Nelson, Phys. Rev. Lett. 41, 121, 519(E) (1978); D. R. Nelson and B. I. Halperin, *ibid.* 19, 2457 (1979).
[9]C. H. Bennett, J. Appl. Phys. 43, 2727 (1972).
[10]J. L. Finney, Proc. R. Soc. (London) Ser. A 319, 479 (1970); 319, 495 (1970).
[11]See, e.g., R. Collins, *Phase Transitions and Critical Phenomena,* edited by C. Domb and M. S. Green (Academic, New York, 1972), Vol. II.
[12]R. Pindak, D. E. Moncton, S. C. Davey, and J. W. Goodby, Phys. Rev. Lett. 46, 1135 (1981).
[13]In the early stages of the Bennett construction there will be ambiguity in placing the next disk, due to the reflection symmetry of the seed. This degeneracy is broken either by roundoff errors, or by some convention in the computer program.
[14]N. D. Mermin, Rev. Mod. Phys. 51, 591 (1979).
[15]P. Collet and J. P. Eckmann, *Iterated Maps of the Interval as Dynamical Systems* (Birkhäuser, Cambridge, Mass., 1980).
[16]J. P. McTague, D. Frenkel, and G. Allen, in *Proceedings of the Conference on Ordering in Two Dimensions,* edited by S. Sinha (North-Holland, Amsterdam, 1980).
[17]It can easily be shown that the diameter ratio corresponding to n disks packed perfectly around a central disk is

$$R=\left[\frac{1}{\sin\pi/n}-1\right]^{\pm 1},$$

where the + applies to $n=3,4,5$, and the − to $n=7,8,9,\ldots$. $R=1$ for $n=6$.